



Contents lists available at ScienceDirect

## International Journal of Coal Geology

journal homepage: [www.elsevier.com/locate/ijcoalgeo](http://www.elsevier.com/locate/ijcoalgeo)

## Permeability evolution in fractured coal: The roles of fracture geometry and water-content

Shugang Wang<sup>a,\*</sup>, Derek Elsworth<sup>a</sup>, Jishan Liu<sup>b</sup>

<sup>a</sup> Department of Energy and Mineral Engineering, EMS Energy Institute and G<sup>3</sup> Center, Pennsylvania State University, University Park, PA, USA

<sup>b</sup> School of Mechanical Engineering, The University of Western Australia, WA, Australia

### ARTICLE INFO

#### Article history:

Received 19 January 2011  
Received in revised form 13 April 2011  
Accepted 15 April 2011  
Available online 1 May 2011

#### Keywords:

Permeability evolution of coal  
Fracture geometry  
Water-content  
Sorption  
Swelling strain

### ABSTRACT

We report laboratory experiments that investigate the permeability evolution of an anthracite coal as a function of applied stress and pore pressure at room temperature as an analog to other coal types. Experiments are conducted on 2.5 cm diameter, 2.5–5 cm long cylindrical samples at confining stresses of 6 to 12 MPa. Permeability and sorption characteristics are measured by pulse transient methods, together with axial and volumetric strains for both inert (helium (He)) and strongly adsorbing (methane (CH<sub>4</sub>) and carbon dioxide (CO<sub>2</sub>)) gases. To explore the interaction of swelling and fracture geometry we measure the evolution of mechanical and transport characteristics for three separate geometries – sample A containing multiple small embedded fractures, sample B containing a single longitudinal through-going fracture and sample C containing a single radial through-going fracture. Experiments are conducted at constant total stress and with varied pore pressure – increases in pore pressure represent concomitant (but not necessarily equivalent) decreases in effective stress. For the samples with embedded fractures (A and C) the permeability first decreases with an increase in pressure (due to swelling and fracture constraint) and then increases near-linearly (due to the over-riding influence of effective stresses). Conversely, this turnaround in permeability from decreasing to increasing with increasing pore pressure is absent in the discretely fractured sample (B) – the influence of the constraint of the connecting fracture bridges in limiting fracture deformation is importantly absent as supported by theoretical considerations. Under water saturated conditions, the initial permeabilities to all gases are nearly two orders of magnitude lower than for dry coal and permeabilities increase with increasing pore pressure for all samples and at all gas pressures. We also find that the sorption capacities and swelling strains are significantly reduced for water saturated samples – maybe identifying the lack of swelling as the primary reason for the lack of permeability decrease. Finally, we report the weakening effects of gas sorption on the strength of coal samples by loading the cores to failure. Results surprisingly show that the strength of the intact coal (sample A) is smaller than that of the axially fractured coal (sample B) due to the extended duration of exposure to CH<sub>4</sub> and CO<sub>2</sub>. Average post-failure particle size for the weakest intact sample (A) is found to be three times larger than that of the sample B, based on the sieve analyses from the samples after failure. We observe that fracture network geometry and saturation state exert important influences on the permeability evolution and strength of coal under in situ conditions.

© 2011 Elsevier B.V. All rights reserved.

### 1. Introduction

Gas transport in coal seams is significantly different from that of other rock types because of the phenomena of gas sorption and coal swelling. The relative roles of stress level, gas pressure, gas composition, fracture geometry of coal, and water content are intimately connected to the processes of gas sorption, diffusion, transport, and coal swelling. Scientific research on coal–gas interactions has been conducted for more than a century, but the physicochemical and hydro-thermodynamic phenomena

are still not fully understood. Understanding and quantifying these interactions is essential in developing the best possible process-based models of behavior that incorporate key observed responses. This characterization is important in preventing gas outbursts in coal mines, in predicting CO<sub>2</sub> injectability into coal seams and in estimating the long-term stability of CO<sub>2</sub> sequestered in coal beds.

Significant experimental effort has been applied to investigate gas permeability and its evolution in coal. Laboratory measured permeabilities of coal to sorbing gases such as CH<sub>4</sub> and CO<sub>2</sub> are known to be lower than permeabilities to nonsorbing or lightly sorbing gases such as argon and nitrogen (N<sub>2</sub>) (Siriwardane et al., 2009; Somerton et al., 1975). Permeabilities may decrease by as much as five orders of magnitude for confining pressures increasing from 0.1 to 70 MPa (Durucan and Edwards, 1986; Huy et al., 2010; Somerton et al., 1975).

\* Corresponding author at: 230A Hosler Building, Penn State University, University Park, PA, 16802, USA. Tel.: +1 814 321 5291; fax: +1 814 865 3248.

E-mail address: [szw138@psu.edu](mailto:szw138@psu.edu) (S. Wang).

Under constant total stress, sorbing gas permeability decreases with increasing pore pressure due to coal swelling (Mazumder and Wolf, 2008; Pan et al., 2010; Robertson and Christiansen, 2005; Wang et al., 2010b), and increases with decreasing pore pressure due to matrix shrinkage (Cui and Bustin, 2005; Harpalani and Chen, 1997; Harpalani and Schraufnagel, 1990; Seidle and Huitt, 1995). Rebound pressure, which corresponds to the minimum permeability, has been observed for CO<sub>2</sub> injection at 1.7 MPa (Pini et al., 2009), and at 7 MPa (Palmer and Mansoori, 1996; Shi and Durucan, 2004). Permeability of sorbing gas in coal is found to be a function of gas exposure time (Siriwardane et al., 2009). Permeability is also influenced by both the presence of water and the magnitude of water saturation (Han et al., 2010). Based on field and laboratory experimental results, several permeability models have been developed for coal seams (Cui and Bustin, 2005; Izadi et al., 2011; Liu and Rutqvist, 2010; Palmer and Mansoori, 1998; Pekot and Reeves, 2002; Seidle and Huitt, 1995; Shi and Durucan, 2005; Wang et al., 2009; Zhang et al., 2008).

The sorption capacities of coal to N<sub>2</sub>, CH<sub>4</sub> and CO<sub>2</sub> have been explored using a variety of measurement methods. Experiments have shown that CO<sub>2</sub> is adsorbed preferentially relative to CH<sub>4</sub> in most instances, and the ratios of the sorption capacities (in molar units) are between 1.15 and 3.16 (Bae and Bhatia, 2006; Battistutta et al., 2010; Busch et al., 2003; Clarkson and Bustin, 1999; Harpalani et al., 2006; Li et al., 2010; Mastalerz et al., 2004; Ottiger et al., 2008). This ratio decreases with increasing temperature (Bae and Bhatia, 2006; Li et al., 2010). The sorption capacity ratios of CO<sub>2</sub> to N<sub>2</sub> are found to be between 2:1 and 8.5:1 (Battistutta et al., 2010; Saghafi et al., 2007; Shimada et al., 2005). However, some coals under certain conditions show a larger sorption capacity to CH<sub>4</sub> than to CO<sub>2</sub> (Busch et al., 2003; Busch et al., 2006; Majewska et al., 2009). The presence of water reduces the sorption capacity to gases by around 30% (Gruskiewicz et al., 2009; Kelemen and Kwiatek, 2009; Siemons and Busch, 2007), due to the competition between water molecules and the sorbing gas for sorption sites on the coal surface (Busch et al., 2007; van Bergen et al., 2009). Applied stress can reduce the sorption capacity of coal by 5%–50% (Hol et al., 2011). Sorption and swelling processes have been shown to be heterogeneous in coal (Day et al., 2008; Karacan, 2003; Karacan, 2007; Karacan and Okandan, 2001) as apparent from quantitative X-ray CT imaging and from optical methods.

Previous studies have shown that coal swells when exposed to N<sub>2</sub>, CH<sub>4</sub>, and CO<sub>2</sub>, with volumetric strain ranging from 0.1% to 15%, under pressures up to 20 MPa and temperatures up to 55 °C (Cui et al., 2007; Day et al., 2008; Harpalani and Schraufnagel, 1990; Karacan, 2007; Kiyama et al., 2011; Levine, 1996; Mazumder and Wolf, 2008; Robertson and Christiansen, 2005; Seidle and Huitt, 1995; Wang et al., 2010a,b). Coal swelling strain increases with increasing pore pressure and strain induced by CO<sub>2</sub> is commonly larger than that induced by CH<sub>4</sub>. The swelling strain is either reversible (Battistutta et al., 2010; Day et al., 2008; Levine, 1996) or irreversible (Czerw, 2011; Majewska et al., 2010). The relation between swelling strain and the amount or volume of gas sorbed is found to be either linear (Chikatamarla et al., 2004; Cui et al., 2007; Czerw, 2011; Levine, 1996; Robertson and Christiansen, 2005) or non-linear (Day et al., 2008; Kelemen and Kwiatek, 2009; Majewska et al., 2010). Coal swelling strain of wet coals is less than that of dry coals (Kiyama et al., 2011; Mazumder and Wolf, 2008; van Bergen et al., 2009), illustrating the effect of water on the swelling strain.

The effect of sorption on the mechanical strength and structure of coal has also been previously investigated. Weakening due to the introduction of CO<sub>2</sub> to a coal is found in uniaxial compression tests (Ranjith et al., 2010; Viete and Ranjith, 2006). In some cases, no evidence of coal weakening is found to result following gas sorption (Ates and Barron, 1988; Day et al., 2008; Pan et al., 2010) even though the sorption process may alter the pore structure of the coal (Goodman et al., 2005; Larsen, 2004; Liu et al., 2010).

Gas transport in coal seams is commonly represented as a dual porosity system accommodating two serial transport mechanisms: diffusion through the coal matrix then laminar flow through the

cleat system (Bai and Elsworth, 2000; Elsworth and Bai, 1992). The permeability is primarily determined by the cleat aperture (Wu et al., 2010a, b; Zhang et al., 2008). The change in cleat aperture is a function of effective stress through poroelasticity (Izadi et al., 2011; Wu et al., 2010a, b). Meanwhile, coal swelling and shrinkage under a confining stress may also change the cleat aperture (Izadi et al., 2011; Wu et al., 2010a, b). Thus, the net change in coal permeability is a function of both the poroelastic response and the coal swelling or shrinkage. To explore the evolution of permeability due to coal swelling we report systematic experiments on three samples with different fracture geometries: 1) sample A containing multiple small embedded fractures, 2) sample B with a longitudinal through-going fracture, and 3) sample C with a radial through-going fracture. This suite of three scenarios simply represents the end members of the effect of fracture geometry on the evolution of permeability in reservoirs in the field. This paper presents experimental results for an anthracite coal under both dry and water saturated conditions at room temperature for these three samples. In this study a triaxial cell is used to measure gas (He, CH<sub>4</sub>, and CO<sub>2</sub>) permeability, sorption, swelling, and strength of coal cores at a series of pore pressures up to 6 MPa and confining pressures up to 12 MPa.

## 2. Experimental method

### 2.1. Experimental setup

The measurements presented in this study are recovered from a standard triaxial apparatus arranged for flow-through or pulse permeability testing as shown in Fig. 1. A triaxial core holder (Temco) is capable of accepting membrane-sheathed cylindrical samples (2.5 cm diameter and 5 cm long) and of applying independent loading in the radial and axial directions. Confining and axial stresses up to 35 MPa are applied by a dual cylinder syringe pumps (ISCO 500D) with control up to  $\pm 0.007$  MPa. Constant upstream pressure can be applied by a third syringe pump (ISCO 500D) with the downstream reservoir open to the atmosphere to measure both water and gas permeabilities to  $10^{-23}$  m<sup>2</sup>. The syringe pumps used to control pressure, consist of a piston-cylinder assembly with a maximum internal volume of 507.38 ml, that can be operated either in constant pressure mode (up to 35 MPa), or constant flow rate mode (up to 204 ml min<sup>-1</sup>), or constant volume mode (up to 507.38 ml). Volume changes in the pore fluid system can be derived from the pump displacement calculated from stepper-motor drive increments (resolution 31.71 nl). A temperature control jacket is used to maintain constant temperature of 0.1 °C. Axial strain is measured by a linear variable displacement transducer (LVDT, Trans-Tek 0244) to a resolution of  $\pm 1$   $\mu\epsilon$  and volumetric strain is measured by volume change in the confining fluid also to  $\pm 1$   $\mu\epsilon$ .

The cylindrical sample is sandwiched within the Temco core holder between two cylindrical stainless steel loading platens with through-going flow connections and flow distributors. The sample and axial platens are isolated from the confining fluid by a polyvinyl chloride (PVC) rubber jacket. The end-platens are connected to two low-volume stainless steel gas reservoirs through tubing and isolating valves when the pressure transient method is applied to measure permeability. The volumes of these interchangeable upstream and downstream reservoirs are 17.36 cm<sup>3</sup> and 3.1 cm<sup>3</sup>, respectively. Upstream and downstream fluid pressures are measured by pressure transducers (PDCR 610 and Omega PX302-5KGV) to a resolution of 0.03 MPa. The gas-pressurized upstream reservoir is discharged through the sample to the downstream reservoir with equilibration time defining permeability of the sample (Brace et al., 1968; Hsieh et al., 1980). Volume change effects due to the high compressibility of gas in the reservoirs are minimized by immersing the gas reservoirs in water baths to maintain constant temperature. The mass of gas sorbed into the coal samples is calculated from mass balance.

Pressure, flow rate, and fluid volume signals obtained from the ISCO pumps are recorded using a National Instruments Labview program and a

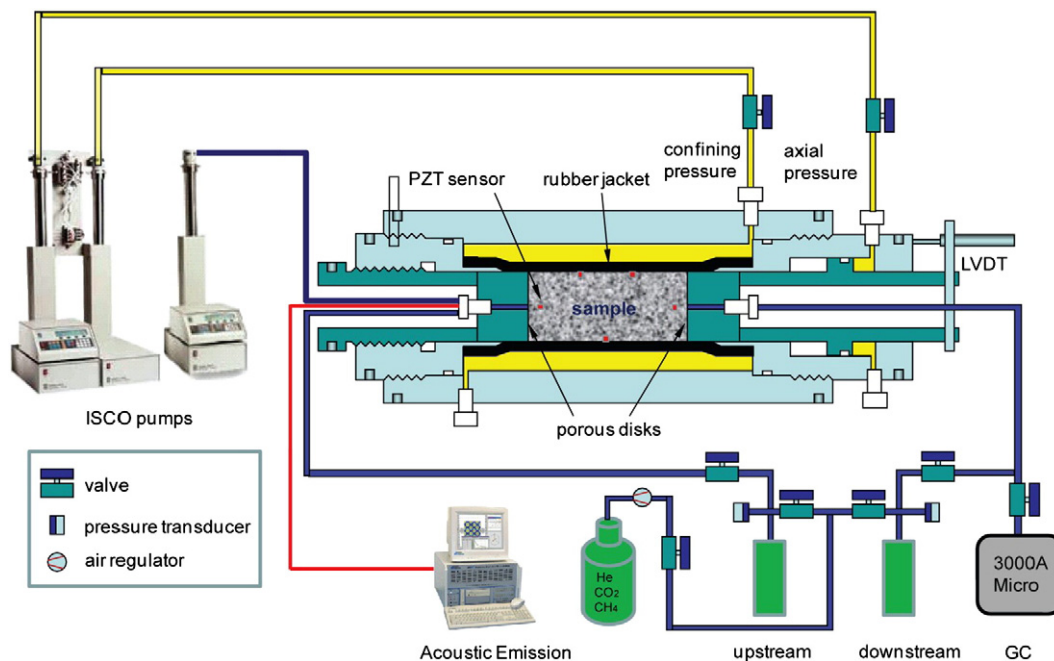


Fig. 1. Schematic of the experimental setup.

serial connection (RS-232) between the pumps and the logging computer. Output signals from a single LVDT and two pressure transducers are converted at 16-bit resolution using a 16-channel data acquisition system (National Instruments – USB 6211). The signals are then logged digitally at a sampling rate from 1 Hz to 1 kHz by a computer using Labview.

The Temco triaxial cell stiffness is first calibrated in order to obtain the true sample deformation when samples are loaded. We calibrate the apparatus with a stainless steel dummy-sample with a known Young's modulus, loaded axially in the core holder at conditions identical to those used in the experiments on coal samples. For each gas permeability test a He leak check is first conducted to make sure there is no leak in the system prior to loading. The fidelity of permeability measurement in this apparatus was also verified through comparison with measurements on a low-permeability calibration sample (in this particular case for granite).

## 2.2. Sample preparation

The experiments were performed on anthracite coal from the Northumberland Basin, Mount Carmel, Pennsylvania recovered as a large block from a depth of 122 m. Samples A and B were drilled parallel to the bedding plane, while sample C was drilled perpendicular to the bedding plane. A roughness of 3 on Barton's scale is estimated for bedding planes in this coal. The cleat aperture is approximately 10–50 μm. The mean density of the coal under unconfined conditions was calculated from the mass and volume of the three cylindrical cores. This procedure yielded an average matrix density of 1397.9 kg m<sup>-3</sup>. Table 1 summarizes the properties of the coal. The pure gases used in this study are CO<sub>2</sub> and CH<sub>4</sub> at purities of 99.995% and He at a purity of 99.999%.

X-ray diffraction (XRD) confirms that kaolinite, quartz, illite, rutile, pyrite, and calcite are the mineral compositions in the coal. The coal does not contain swelling clay minerals, such as smectite, montmorillonite, and hectorite. Hence, the effect of clay swelling on the swelling strain of coal under water-saturated conditions is negligible.

## 2.3. Measurement procedure

Conventional triaxial experiments are used to concurrently measure permeability, sorption, deformability and strength of the sample coals under recreated in situ conditions of applied stress.

### 2.3.1. Permeability

For experiments conducted under dry condition, samples are placed in an oven at 40 °C under vacuum for 24 h before being placed in the triaxial cell. For tests performed under water saturated conditions, a 3 MPa constant upstream pressure is first applied by the third ISCO pump for 24 h with the downstream reservoir open to the atmosphere. After the samples are saturated we disconnect the ISCO pump and apply the same procedure for dry samples under the same conditions.

We use the pressure transient method to conduct the gas flow experiments in the low permeability samples (Brace et al., 1968; Hsieh et al., 1980). In a typical experiment, the sample is placed into the triaxial core holder and both confining stress and axial stresses are

Table 1  
Properties of the used Pennsylvania anthracite coal.

Proximate analysis					
Fixed carbon	Volatile matter		Ash		
86.3%	7.37%		3.60%		
Ultimate analysis					
Carbon	Hydrogen	Nitrogen	Sulfur	Oxygen	
93.1%	3.1%	1.0%	0.5%	2.3%	
Maceral composition (Pappano, et al., 1999)					
Vitrinite	Fusinite	Semi-fusinite	Liptinite	Liptinite	
60%	24%	14%	1%	1%	
Constituent of mineral matter					
Kaolinite	Quartz	Illite	Pyrite	Rutile	Calcite
72.6%	11.0%	5.0%	5.3%	3.2%	2.9%
Sample physical properties					
Sample	Length (cm)	Porosity (%)	Water content (wt.%) (saturated condition)		
A	4.67	2.0	1.4		
B	5.00	3.4	2.5		
C	5.31	2.7	1.9		

applied at a rate of 5 MPa/min to establish initial conditions and are then kept constant. The sample-reservoir system is then vacuum desaturated to evacuate air from the system. A pressure increment is then applied to the upstream gas reservoir and discharged through the sample to the downstream gas reservoir. The time taken for the discharging upstream reservoir and the recharging downstream reservoir to reach a new equilibrium pressure is measured. This pattern is repeated for multiple cycles using the desired gas permeant. After multiple repeats of this procedure a relation between permeability and pore pressure and effective stress is obtained. In this work, confining pressures range between 6 and 12 MPa, and gas reservoir pressures are in the range 1 to 6 MPa. The pressure decay rate recorded in the upstream reservoir and the pressure increase rate in the downstream reservoir are used to evaluate permeability. The decay characteristics depend on the permeability, on the dimensions of the sample and reservoirs, and on the physical characteristics of the permeating fluid.

The experimental and analytical details of the pressure transient method for determining permeability can be found elsewhere (Brace et al., 1968; Hsieh et al., 1980). However, the governing equation for the pressure pulse through the coal sample can be written as follows.

$$P_{up}(t) - P_{dn}(t) = (P_{up}(t_0) - P_{dn}(t_0)) e^{-\alpha t} \quad (1)$$

$$\alpha = (kA / \mu\beta L) (1 / V_{up} + 1 / V_{dn}) \quad (2)$$

where  $P_{up}(t) - P_{dn}(t)$  is the pressure difference between the upstream and downstream reservoirs at time  $t$ ; and  $(P_{up}(t_0) - P_{dn}(t_0))$  is the initial pressure difference between the upstream and downstream reservoirs at time  $t_0$ .  $\alpha$  is the slope of the line when plotting the pressure decay  $P_{up}(t) - P_{dn}(t)$  on semi-log paper against time.  $A$  and  $L$  are the cross-sectional area and length of the sample, respectively, which define the dimensions of the sample.  $\mu$ ,  $\beta$ ,  $V_{up}$ , and  $V_{dn}$  are the dynamic viscosity and compressibility of the gas, and the volume of the upstream reservoir and downstream reservoir, respectively. Permeability  $k$  is calculated from Eq. (2) where it is the only unknown.

### 2.3.2. Sorption

We measure the void volume of the sample as a direct consequence of measuring the permeability to He using the pressure transient method. We first vacuum desaturate the sample-reservoir system to evacuate air from the system and inject a known amount of He to the upstream and then open the shut-off valve. Since He is inert, the void volume can be calculated from the pressures of the upstream and downstream reservoirs and cell, and the volumes from upstream and downstream reservoirs, as shown in Eq. (3).

$$\left( P_{up} V_{up} / ZRT \right)_{pulse,10} = \left( P(V_{up} + V_{dn} + V_{vd}) / ZRT \right)_{pulse,1} \quad (3)$$

where the subscript  $pulse,10$  denotes the initial condition for the pressure pulse 1 and subscript  $pulse,1$  represents the final condition for the pressure pulse 1,  $Z$  is the compressibility factor of the gas at corresponding temperature and pressure,  $R$  is the universal gas constant,  $T$  is the absolute temperature,  $P$  is the final pressure of the system, and  $V_{vd}$  is the unknown void volume of the sample corresponding to pressure pulse 1.

We repeat this procedure for multiple cycles and then we obtain the void volume of the sample corresponding to different pressures.

$$\left( P_{up} V_{up} / ZRT \right)_{pulse,n0} + (P(V_{dn} + V_{vd}) / ZRT)_{pulse,n-1} = \left( P(V_{up} + V_{dn} + V_{vd}) / ZRT \right)_{pulse,n} \quad (4)$$

where subscript  $pulse,n0$  denotes the initial condition for the pressure pulse subscripts  $n$  and  $pulse,n$  represents the final condition for the  $n$ th pressure pulse.

After obtaining the void volume of the sample at different pressures, we run the same tests using  $CH_4$  and  $CO_2$ . Since  $CH_4$  and  $CO_2$  are sorbing gases, the mass balance equation can be expressed as follows.

$$\left( P_{up} V_{up} / ZRT \right)_{pulse,n0} + (P(V_{dn} + V_{vd}) / ZRT)_{pulse,n-1} = \left( P(V_{up} + V_{dn} + V_{vd}) / ZRT \right)_{pulse,n} + n_{pulse,n} \quad (5)$$

where  $n_{pulse,n}$  is the amount of gas adsorbed in the sample in moles for the  $n$ th pressure pulse.

These steps are repeated until the desired final pressure level is reached. The cumulative amount of gas adsorbed in the sample can be calculated by summing up the quantities measured in each pressure pulse step. Gas properties for He,  $CH_4$  and  $CO_2$  are calculated from the NIST webbook at <http://webbook.nist.gov/chemistry/fluid/>.

### 2.3.3. Swelling strain

We measure the swelling strain that evolves during the permeability measurement as described above on the same coal samples. An LVDT is used to measure the axial strain of the sample. Correction is made on the axial strain due to the effect of the elastic stiffness of the triaxial cell. Radial strain is measured from the volume change of the confining fluid in the ISCO pump with subtraction of the effects of sample axial deformation and compression of the rubber jacket. For each sample, we first measure the volumetric strain  $\epsilon_{pulse,n}^{He}$  induced by He injection at different pressures. Under constant total stress, the injection of He leads to expansion of the coal sample. Since He is a non-sorbing gas, this volumetric strain is only due to the poroelastic effect. Then we measure the volume strain  $\epsilon_{pulse,n}^{CH_4}$  and  $\epsilon_{pulse,n}^{CO_2}$  induced by  $CH_4$  and  $CO_2$  injection at the same pressures. Finally, we obtain the swelling strains  $\epsilon_{pulse,n}^{CH_4,sw}$  and  $\epsilon_{pulse,n}^{CO_2,sw}$  for  $CH_4$  and  $CO_2$  at these pore pressures, as expressed in Eqs (6) and (7), appropriately separated for each of the permeating gases.

$$\epsilon_{pulse,n}^{CH_4,sw} = \epsilon_{pulse,n}^{CH_4} - \epsilon_{pulse,n}^{He} \quad (6)$$

$$\epsilon_{pulse,n}^{CO_2,sw} = \epsilon_{pulse,n}^{CO_2} - \epsilon_{pulse,n}^{He} \quad (7)$$

### 2.3.4. Strength

In order to investigate the effect of sorption on the strength of the samples we stress the samples to failure immediately after the full suite of permeability and sorption measurements are completed. Samples are  $CO_2$  saturated for 24 h with effective confining pressure at 1 MPa. We apply a constant strain rate of  $2 \times 10^{-5} s^{-1}$  until failure to obtain a preliminary indication of the effects of sorption on coal strength. We run a sieve analysis of the broken particles of the samples as percent weight to check the particle size distribution for sieve sizes of 9.5 mm, 6.35 mm, 4.76 mm, 3.36 mm, 2.83 mm, 1.68 mm, 1 mm, and 0.42 mm, and 0.21 mm. The average particle size is calculated based on Eq (8),

$$D = \sum_{i=1}^9 m_i d_i / m \quad (8)$$

where  $D$  is the average particle size,  $m_i$  is the mass of the  $i$ th opening, and  $d_i$  is the size of the  $i$ th opening, and  $m$  is the total mass of the broken sample.

## 3. Experimental observation

Measurements of the evolution of permeability, sorption, and swelling strain to permeation by He,  $CH_4$ , and  $CO_2$  are presented together with coal triaxial strengths and post failure particle size distribution. All experiments are conducted at room temperature. We define effective stress as the difference between confining stress and pore pressure inside the sample (Biot coefficient of unity).

In particular, experiments of permeability, sorption, and swelling are conducted for two different sets of conditions. These conditions are: (1) constant confining and constant axial stresses with increasing gas pressure, and (2) constant gas pressure with increasing confining and axial stresses. The influence of effective-stress-driven changes in volumes are examined with non-sorbing He as the permeant. The superposed influence of swelling is examined with the sorbing gases CH<sub>4</sub> and CO<sub>2</sub>. We report these results sequentially for the cleat-fractured sample (sample A) and for samples containing discrete fractures in the axial (sample B) and transverse (sample C) directions. The schematic of these three samples is shown in Fig. 2.

3.1. Results for the ubiquitously fractured sample (sample A)

3.1.1. Dry sample

Sample A contains multiple small embedded fractures. Permeability evolution measured with respect to pore pressure at constant total stresses of 6 MPa and 12 MPa is shown in Fig. 3(a). Under both confining pressures the permeability is highest for He and decreases (for all pore pressures) successively for CH<sub>4</sub> then further for CO<sub>2</sub>. For the same gas permeant, permeability reduces by an order of magnitude as loading is incremented from 6 MPa to 12 MPa. At both stresses, permeabilities of He show an increase in permeability with increasing pore pressure. At 6 MPa total stress the permeability to He increases by 1 order as pore pressure is incremented from 1.44 MPa to 4.24 MPa (i.e. a factor of 3.13 per MPa). At increased stress (12 MPa) this rate of permeability increase reduces to a factor of 0.77 per MPa – likely reflecting the increased stiffness of the cleats at higher stress. At a total stress of 6 MPa, permeabilities measured using CH<sub>4</sub> and CO<sub>2</sub> show a different trend, where permeabilities first decrease and then recover as pore pressure increases above a threshold Langmuir pressure. Under constant total stresses an increase in pore pressure tends to widen the cleats and therefore increase the permeability. However, adsorption-induced coal swelling narrows the cleats, leading to a reduction in permeability. The net change in permeability depends on the net effect. The results in Fig. 3 (a) indicate that as pore pressure increases the reduction in permeability

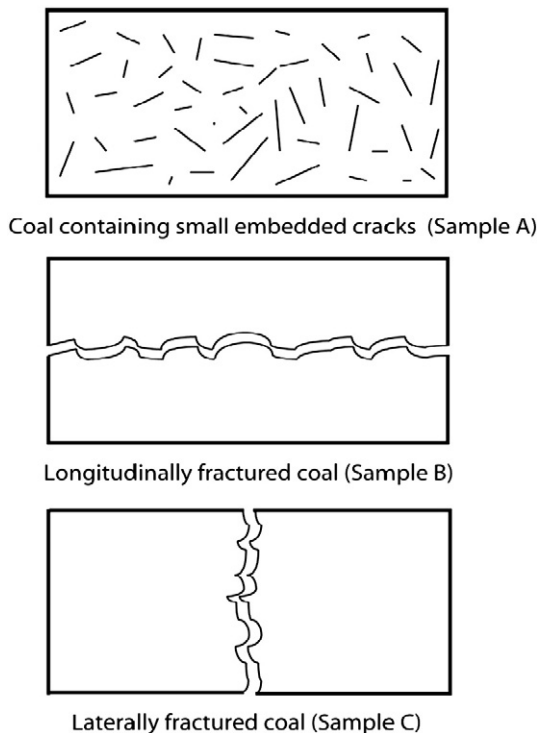


Fig. 2. Schematic of three tested samples.

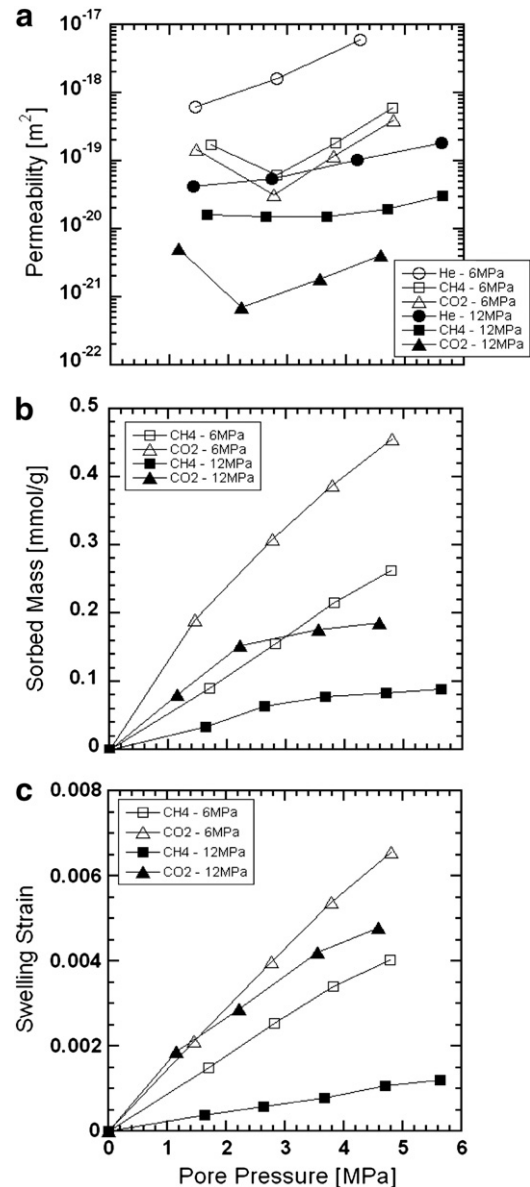


Fig. 3. (a) Evolution of permeability as a function of applied pore pressure for coal with embedded cracks (sample A) for constant applied confining stresses at stepped magnitudes of 6 and 12 MPa. (b) Sorbed mass as a function of applied pore pressure for coal with embedded cracks (sample A) for constant applied confining stresses at stepped magnitudes of 6 and 12 MPa. (c) Swelling strain as a function of applied pore pressure for coal with embedded cracks (sample A) for constant applied confining stresses at stepped magnitudes of 6 and 12 MPa.

driven by coal swelling first dominates the net change of permeability. However, for Langmuir-type swelling, the swelling rate gradually decreases as pore pressure reaches the Langmuir pressure. The effect of permeability increase with the reduction in effective stresses ultimately supercedes the influence of swelling. Permeability of CH<sub>4</sub> first decreases by 65% over a pore pressure of 1.7 to 2.8 MPa, then rebounds to 3.3 times the initial permeability at a final pore pressure of 4.8 MPa. Permeability of CO<sub>2</sub> first decreases by 78% over the pore pressure range of 1.45 to 2.76 MPa then rebounds to 2.7 times the initial permeability at a final pore pressure of 4.8 MPa. The net permeability change is controlled by the competition of permeability reduction driven by coal swelling and permeability enhancement caused by the decline in effective stress.

At a total stress of 12 MPa the permeability to CH<sub>4</sub> declines by 7% as pore pressure is increased from 1.64 to 3.66 MPa, and increases to 1.85 times the initial permeability at a pore pressure of 5.64 MPa.

The permeability to CO<sub>2</sub> first decreases by 86% (pore pressure of 1.15 to 2.22 MPa) and then rebounds to a net 19% reduction over the initial permeability at the final pore pressure of 4.58 MPa. The initial larger reduction in permeability for CO<sub>2</sub> at both confining pressures indicates the larger coal swelling with CO<sub>2</sub> compared to that with CH<sub>4</sub>, which is verified by the sorption and swelling data shown later in this paper. The influence of effective stress on permeability evolution is shown in Fig. 4 (a). For the same gas permeant, increasing effective stress generally decreases the permeability (Durucan and Edwards, 1986; Somerton et al., 1975; Wu et al., 2010a). The rate of permeability reduction is greatest at low effective stresses. This is consistent with cleat and microfracture stiffnesses that are largest at high closure stresses.

Sorption capacity is measured to CH<sub>4</sub> and CO<sub>2</sub> on this ubiquitously fractured sample (A) at pore pressures up to 5.6 MPa and at total stresses of 6 MPa and 12 MPa and are presented in Fig. 3(b). As pore pressure increases the cumulative sorbed mass increases. All isotherms can be approximately described by Langmuir-type curves. The four curves show distinct differences both in the absolute amount of sorption and in the shapes of the isotherms. The sorption isotherms of the sample under low confining pressure show a gradual increase from the low-pressure range to the high-pressure range. However, the sorption isotherms under high confining stress show a relatively steep increase in the low-pressure range (up to 2.6 MPa) and subsequently approach limiting values, in the 3–5 MPa range. This distinction may indicate that higher applied stress reduces the sorption capacity, as shown previously (Hol et al., 2011). The isotherms of the sample under lower confining stress show significantly higher sorption capacities (0.46 mmol CO<sub>2</sub>/g coal and 0.26 mmol CH<sub>4</sub>/g coal) at the final pressures relative to that under high confining stress (0.18 mmol CO<sub>2</sub>/g coal and

0.095 mmol CH<sub>4</sub>/g coal). The sorption capacity ratios between the lower confining stress and high confining stress are 2.56 and 2.74 for CO<sub>2</sub> and CH<sub>4</sub>, respectively. The sorption capacity ratios between CO<sub>2</sub> and CH<sub>4</sub> are 1.77 at low confining stress and 1.89 at high confining stress.

The swelling strain of coal containing embedded fractures (sample A) under different total stresses is shown as a function of pore pressure in Fig. 3(c). We observe that the relationship between the measured swelling and pore pressure is close to linear at low stress and slightly Langmuir-like at elevated stress. Under both confining stresses, the sample exhibits a larger swelling strain when adsorbing CO<sub>2</sub>. For the same gas permeant, at higher confining stress, the swelling strain is reduced, which corresponds to the fact that the sample is relatively stiffer at higher confining stress. At a total stress of 6 MPa, the swelling strain due to CO<sub>2</sub> adsorption is 0.65% and due to CH<sub>4</sub> adsorption is 0.4% at a pore pressure 4.8 MPa. The ratio of swelling strain between CO<sub>2</sub> and CH<sub>4</sub> at a total stress of 6 MPa is 1.625. At a total stress of 12 MPa, the swelling strains are 0.48% and 0.12% for CO<sub>2</sub> and CH<sub>4</sub> sorption respectively, with a ratio of 4. The swelling strain decreases by 27% due to CO<sub>2</sub> adsorption and by 69% due to CH<sub>4</sub> adsorption as confining pressure increases from 6 MPa to 12 MPa. This smaller reduction in swelling for CO<sub>2</sub> indicates that at higher total stress the sample is easier to swell due to CO<sub>2</sub> sorption than due to CH<sub>4</sub> sorption. This may result since CO<sub>2</sub> can be preferentially adsorbed into smaller pores (i.e., <0.31 nm) because of the higher adsorption affinity (energy) (Cui et al., 2004).

The relationship between swelling strain and effective stress is shown in Fig. 4(b). The rate of gas uptake at higher strain is smaller than at lower strains – representing behaviors at low and high stresses. This is consistent with the sample being stiffer at higher effective stresses and the swelling strain having to react against bridging asperities in generating swelling deformations.

The relationship between the amount of gas adsorbed in coal containing embedded fractures (sample A) as a function of swelling strain is displayed in Fig. 5. We observe that the relation between sorbed mass and swelling strain is approximately linear at a confining stress of 6 MPa for both CH<sub>4</sub> and CO<sub>2</sub>. At a confining stress of 12 MPa, for both CH<sub>4</sub> and CO<sub>2</sub> adsorption slows at pore pressures above 3 MPa but swelling continues, consistent with prior observations in the literature (Bustin, 2004; Levine, 1996). This behavior may be explained by the fact that both sorption and swelling are time-dependent, but with a much slower rate in swelling at a higher confining pressure. We also notice the difference in the slope of the curves under different confining pressures. For the sorption of CH<sub>4</sub> a similar slope is exhibited throughout the pressure range. The larger amount of gas adsorbed is presumably needed for the same amount of swelling at a high confining pressure for CH<sub>4</sub>, which may imply a higher stiffness at high confining pressure. However, the total swelling strain at higher confining pressure is even less than that of the first pressure step at lower confining pressure. No clear conclusion can be drawn from the slope difference for CH<sub>4</sub>. For the sorption of CO<sub>2</sub> and for the same amount of gas adsorbed, larger swelling strain is shown at a higher confining pressure for CO<sub>2</sub>, which may be the sign of the weakening effect of CO<sub>2</sub>.

### 3.1.2. Water-saturated sample

For comparison the evolution of permeability of the ubiquitously fractured sample (sample A) under dry and water-saturated conditions at a total stress 6 MPa is shown in Fig. 6(a). Under water-saturated condition, He has the largest permeability, and is followed progressively by CH<sub>4</sub> and CO<sub>2</sub>. This progression of permeability magnitudes is the same as in tests under dry condition. However, the initial permeabilities of wet samples are uniformly reduced by two orders of magnitude over the dry samples – indicating the role of water in occluding microfractures (Han et al., 2010). Measured permeability with He increases with a higher rate with pore pressure compared with the results under dry condition. However, different from the results from dry samples, no permeability reduction is seen for CH<sub>4</sub> and CO<sub>2</sub> with increasing pore pressure. The presence of water reduces the permeability significantly so the sample

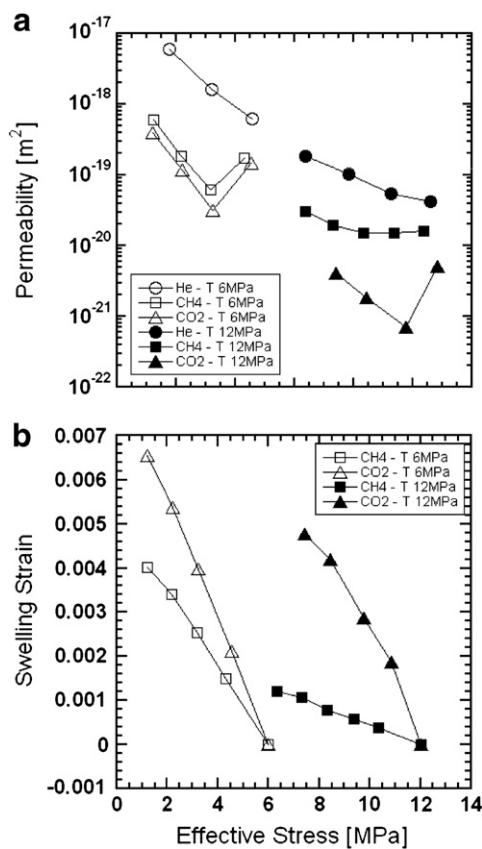


Fig. 4. (a) Evolution of permeability as a function of applied effective stress for coal with embedded cracks (sample A) for constant applied confining stresses at stepped magnitudes of 6 and 12 MPa. (b) Swelling strain as a function of applied effective stress for coal with embedded cracks (sample A) for constant applied confining stresses at stepped magnitudes of 6 and 12 MPa.

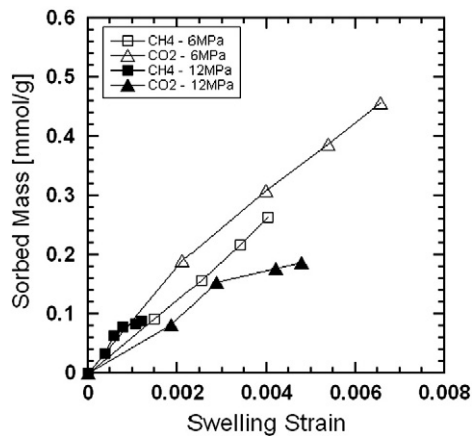


Fig. 5. Sorbed mass as a function of swelling strain for coal with embedded cracks (sample A) for constant applied confining stresses at stepped magnitudes of 6 and 12 MPa.

begins with an extremely low permeability. As pore pressure increases, the amount of water in the sample is gradually displaced by the injected gas, which leads to an increase in permeability. An increment in pore pressure also enhances the permeability due to the influence of decreased effective stresses. At the same time, swelling induced by adsorption with increasing pore pressure lowers the permeability. However, the amount of gas adsorbed and induced swelling are greatly reduced by the presence of water. So the net change in permeability for wet samples depends on the overall effect of these three competitive components. In this case, the permeability enhancement due to effective stress and water displacement dominates the reduction due to coal swelling, showing that permeabilities always increase with pore pressure. This is also consistent with the observation that the rate of change in permeability to He is greater under wet conditions.

The comparison of the sorbed mass as a function of pore pressure of the ubiquitously fractured coal (sample A) under dry and water-saturated conditions at 6 MPa total stress is shown in Fig. 6(b). Sorbed mass is consistently higher for CO<sub>2</sub> versus CH<sub>4</sub> and is reduced by a factor of 3 to 4 when wet versus dry. The isotherms can be approximated by Langmuir-like behavior. At final pressures, the amount of gas adsorbed in the wet sample is reduced by 69% for CO<sub>2</sub> (0.45 mmol/g coal, dry sample; 0.14 mmol/g coal, wet sample) and 69% for CH<sub>4</sub> (0.26 mmol/g coal, dry sample; 0.08 mmol/g coal, wet sample).

Fig. 6(c) compares swelling strain as a function of pore pressure for the coal containing embedded fractures (sample A) under dry and water-saturated conditions at a 6 MPa total stress. As shown before, the measured swelling under dry conditions can be reasonably described by a Langmuir type relationship. The presence of water also reduces the swelling strain by 62% for CO<sub>2</sub> and by 58% for CH<sub>4</sub> at final pressures. The presence of water also makes the initial portion of the curves largely linear and less similar to Langmuir-like behavior. However, at pore pressure above 3 MPa a significant amount of water is displaced by the injected gas and above this stress the swelling strain follows a Langmuir-like relation with pore pressure.

The comparison of the sorbed mass as a function of swelling strain for coal with embedded fractures (sample A) under dry and water-saturated conditions for constant applied confining stress at 6 MPa is shown in Fig. 7. The relation between sorbed mass and swelling strain is approximately linear at confining stress of 6 MPa for both CH<sub>4</sub> and CO<sub>2</sub>. For the same amount of gas adsorbed, the deformation of the sample is generally larger under water-saturated conditions than that under dry conditions for both gases. This may suggest that either a weakening effect of water on the coal sample during CH<sub>4</sub> and CO<sub>2</sub> injection, or the presence of water has a larger negative effect on sorption than swelling.

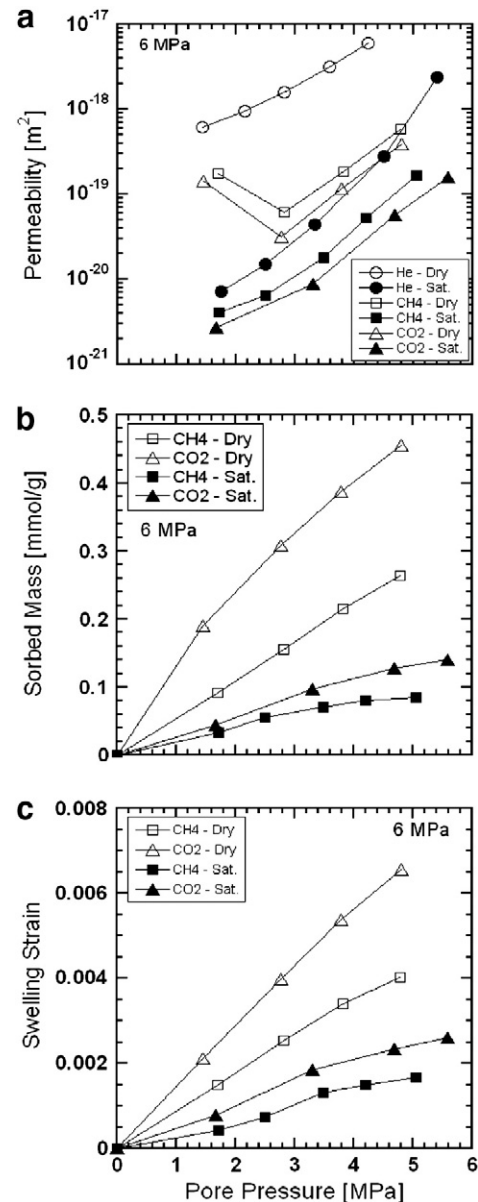


Fig. 6. (a) Comparison of the evolution of permeability as a function of applied pore pressure for coal with embedded cracks (sample A) under dry and water-saturated conditions for constant applied confining stress at 6 MPa. (b) Comparison of the sorbed mass as a function of applied pore pressure for coal with embedded cracks (sample A) under dry and water-saturated conditions for constant applied confining stress at 6 MPa. (c) Comparison of the swelling strain as a function of applied pore pressure for coal with embedded cracks (sample A) under dry and water-saturated conditions for constant applied confining stress at 6 MPa.

### 3.2. Results for the longitudinally fractured sample (sample B)

In this section we show the results for the longitudinally fractured sample (sample B) for both dry and water-saturated conditions. The experiments are completed at a total stress of 6 MPa.

Permeabilities measured with respect to pore pressure at a constant total stress of 6 MPa under both dry and water-saturated conditions are shown in Fig. 8(a). Permeabilities reduce in the succession of He as highest to CO<sub>2</sub> as lowest, as previous. Again, the permeabilities of the water-saturated samples decrease by more than 2 orders of magnitude compared with those of dry samples. Under dry conditions, the ratio in permeability between the longitudinally fractured coal (sample B) and coal containing small embedded fractures (sample A) is more than three

orders of magnitude for all gases. The initial permeabilities of sample B under water-saturated conditions are even higher than that of sample A under dry conditions for each gas. The significant difference in permeabilities of sample A and sample B reflects the important role of fracture geometry. For sample A, we measure the permeability of the coal matrix, while for sample B, we evaluate the permeability of a single longitudinal fracture.

For the same gas permeant He, the rate of increase in permeability due to effective stress is larger for coal with embedded fractures (sample A) than the longitudinally fractured coal (sample B). We also find the rate of change in permeability is higher for the wet sample. Possible reasons are likely to be the same as discussed for sample A.

The relationship between the amount of gas adsorbed in the longitudinally fractured coal (sample B) as a function of pore pressure under both dry and water-saturated condition at a total stress of 6 MPa is shown in Fig. 8(b). For the dry condition, sorbed mass has the same trend as imparted by swelling strain, where the rate of change increases with pore pressure, due to the effect of time dependence. The effect of water is shown again on the sorption capacity of the sample, as the sorption capacities drop by 75% for CH<sub>4</sub> and by 53% for CO<sub>2</sub> from the dry to the wet condition (from 0.072 to 0.018 mmol/g for CH<sub>4</sub>; from 0.097 to 0.046 mmol/g for CO<sub>2</sub>). However, for the wet sample, the relation of the amount of gas adsorbed with pore pressure appears to follow a Langmuir isotherm. This behavior corresponds to the fact that the wet sample has a two order of magnitude lower permeability which increases sorption time by about two orders of magnitude.

The comparison of swelling strain as a function of applied pore pressure of the longitudinally fractured coal (sample B) under dry and water-saturated conditions at a 6 MPa total stress is shown in Fig. 8 (c). The measured swelling under dry condition does not follow the Langmuir-like isotherm. Rather, the rate of change in swelling strain gradually increases with pore pressure. Since sample B has a very high permeability compared with the coal containing small embedded fractures (sample A) it takes much less time (one hundred times faster) to finish a pressure pulse step whereas sorption induced swelling is a time dependent process. It is also evident that the presence of water prevents coal from swelling as the strain is reduced by 28% for CH<sub>4</sub> and by 36% for CO<sub>2</sub>.

The comparison of the sorbed mass as a function of swelling strain for longitudinally fractured coal (sample B) under dry and water-saturated conditions for constant applied confining stress at 6 MPa is shown in Fig. 9. The relation is not linear for both CH<sub>4</sub> and CO<sub>2</sub>. Results show that as pore pressure increases, sorption slows but swelling

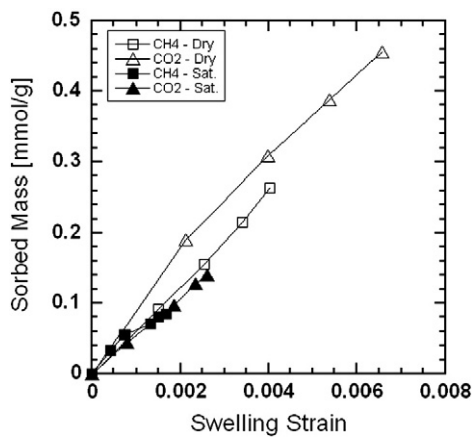


Fig. 7. Comparison of the sorbed mass as a function of swelling strain for coal with embedded cracks (sample A) under dry and water-saturated conditions for constant applied confining stress at 6 MPa.

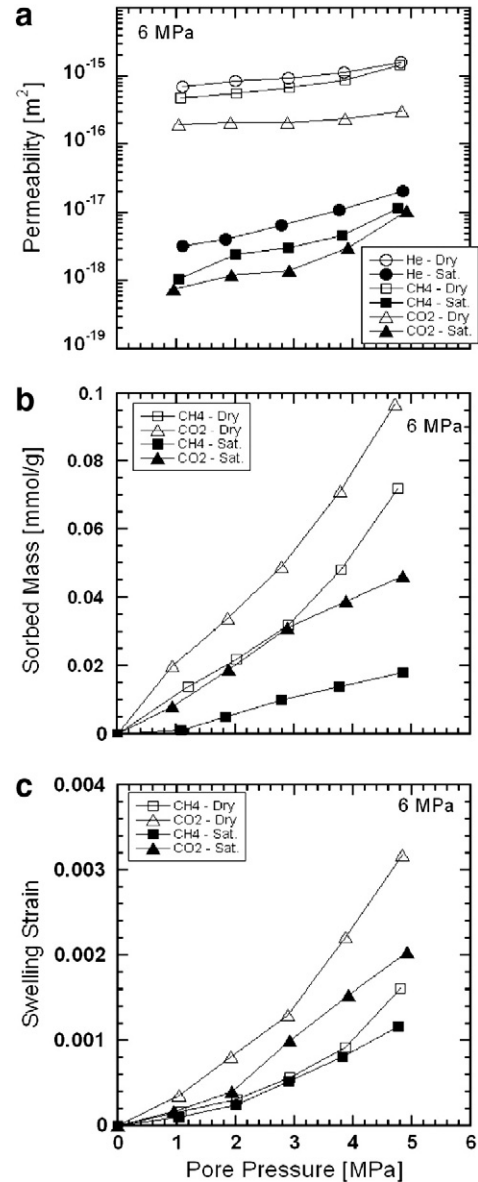


Fig. 8. (a) Comparison of the evolution of permeability as a function of applied pore pressure for longitudinally fractured coal (sample B) under dry and water-saturated conditions for constant applied confining stress at 6 MPa. (b) Comparison of the sorbed mass as a function of applied pore pressure for longitudinally fractured coal (sample B) under dry and water-saturated conditions for constant applied confining stress at 6 MPa. (c) Comparison of the swelling strain as a function of applied pore pressure for longitudinally fractured coal (sample B) under dry and water-saturated conditions for constant applied confining stress at 6 MPa.

continues gradually. Possible reasons are presented in the discussion section in this paper.

### 3.3. Results for the laterally fractured sample (sample C)

In this section, we show the results from sample C with a radial through-going fracture, under both dry and water-saturated conditions at a total stress of 6 MPa.

Permeabilities measured with respect to pore pressure at a constant total stress of 6 MPa under both dry and water-saturated conditions are shown in Fig. 10(a). Under both test conditions, the permeability magnitude is in the order of He, CH<sub>4</sub>, and CO<sub>2</sub>. The initial permeabilities of water-saturated samples decrease significantly compared with that of dry samples. Compared with the initial permeabilities the results for coal containing small embedded fractures (sample A) and a through-going

fracture (B), the permeabilities of the laterally fractured coal (sample C) are closer to sample A. The fracture is perpendicular to flow and has little influence on the transport properties of the sample. Permeability reduction due to the dominant effect of sorption induced swelling is seen again only in the dry sample at lower pore pressures. The presence of water reduced the overall permeability by about one order of magnitude.

The comparison of swelling strain as a function of pore pressure of the laterally fractured coal (sample C) under dry and water-saturated conditions at a total stress of 6 MPa is shown in Fig. 10(c). Under dry condition, the measured swelling strain appears to be a linear function of pore pressure. The sample swells more due to CO<sub>2</sub> adsorption than due to CH<sub>4</sub> adsorption for both conditions (1.8 times more under dry condition, and 2.1 times more under water-saturated condition). It is observed that only a small strain occurs in the first pressure step for both gases under wet condition. Prior results that coal swelling can be induced by water saturation (Walker et al., 1988). During the process of injected gas displacing water, the competition between water and CO<sub>2</sub> molecules may be explained by the less overall swelling of the sample, compared with the value of dry sample. This logic is confirmed by the adsorbed mass of the wet sample shown in Fig. 10(b), where the first sorption step is much less compared with that under dry condition. As pore pressure increases, the water in the sample is gradually displaced by the injected gas, and then sorption and swelling develop at larger rates. It can be inferred from the curves that the majority of water may be displaced after the first pressure pulse step.

The relationship between the amount of gas adsorbed in the laterally fractured coal (sample C) as a function of swelling strain under both dry and water-saturated conditions at a confining stress of 6 MPa shown in Fig. 11. The relation can be approximately described as linear both for CH<sub>4</sub> and for CO<sub>2</sub> under both experimental conditions. As expected, under dry conditions and for the same amount of gas adsorbed, samples with CO<sub>2</sub> deform larger due to the larger coal deformability with CO<sub>2</sub> sorption. The relatively larger swelling strain for wet samples may suggest a water weakening effect again in the laterally fractured coal (sample C).

### 3.4. Strength

The comparison of the strengths of three samples at 1 MPa effective confining pressure and a strain rate of  $2 \times 10^{-5} \text{ s}^{-1}$  is shown in Fig. 12. We find that the strengths are 13.97 MPa, 21.95 MPa, and 21.14 MPa for coal containing small embedded fractures (sample A), the longitudinally

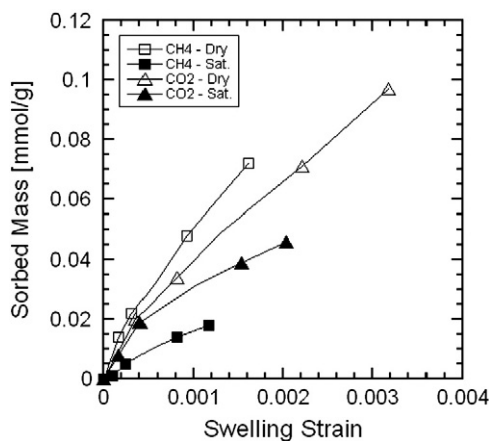


Fig. 9. Comparison of the sorbed mass as a function of swelling strain for longitudinally fractured coal (sample B) under dry and water-saturated conditions for constant applied confining stress at 6 MPa.

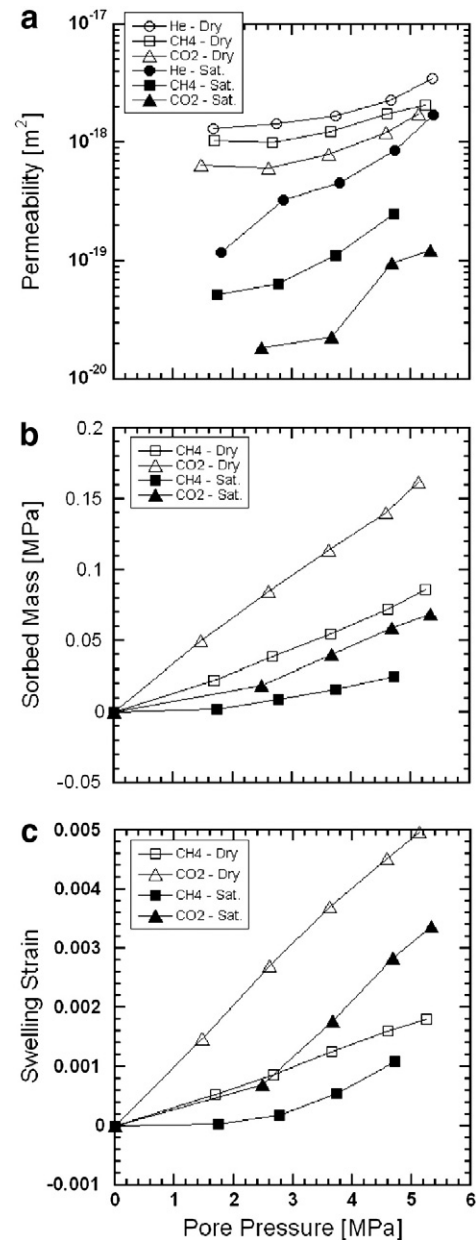


Fig. 10. (a) Comparison of the evolution of permeability as a function of applied pore pressure for laterally fractured coal (sample C) under dry and water-saturated conditions for constant applied confining stress at 6 MPa. (b) Comparison of the sorbed mass as a function of applied pore pressure for laterally fractured coal (sample C) under dry and water-saturated conditions for constant applied confining stress at 6 MPa. (c) Comparison of the swelling strain as a function of applied pore pressure for laterally fractured coal (sample C) under dry and water-saturated conditions for constant applied confining stress at 6 MPa.

fractured coal (sample B), and C, respectively. Samples A and B have exactly the same test conditions, but sample A surprisingly has the lowest strength. This may be attributed to the weakening effects of gas sorption, as shown in the literature on the weakening effect of CO<sub>2</sub> on the strength of coal (Ranjith et al., 2010; Viete and Ranjith, 2006). The time duration for coal containing small embedded fractures (sample A) in a sorptive environment is much longer than that of sample B, due to the significant difference in permeability. This is confirmed by the post-failure sieve analysis. Average post-failure particle sizes are 2.93 mm, 7.59 mm, and 6.47 mm, for sample A, B and C, respectively. The post-failure particle size distribution of three samples is shown in Fig. 13.

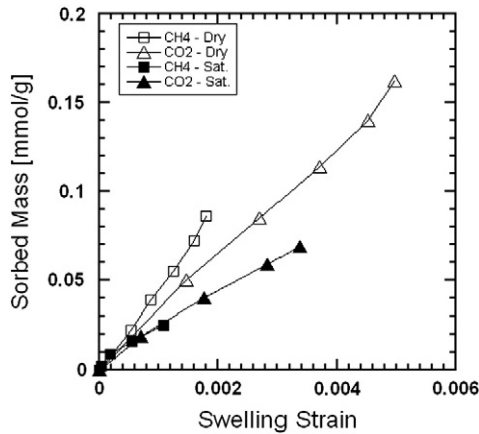


Fig. 11. Comparison of the sorbed mass as a function of applied pore pressure for laterally fractured coal (sample C) under dry and water-saturated conditions for constant applied confining stress at 6 MPa.

#### 4. Discussion

##### 4.1. The role of fracture geometry

Discontinuities such as face cleats and butt cleats are of widespread occurrence. The complexity of fracture networks, especially in their geometry and topology is one major obstruction in developing process-based models for the flow, transport, and mechanical behavior of fractured coal seams. In this paper, we investigate the role of fracture geometry on the flow, sorption, and swelling behavior of anthracite. We compare the results of coal with only small embedded fractures (A) to the behavior of coal with either longitudinal (B) or transverse (C) fractures. These geometries represent end-members of anticipated behavior.

Table 2 summarizes data for permeability, sorption, and swelling strain of coal recovered from the literature. In this study, we find that the permeability of coal containing small embedded fractures (sample A), coal containing a longitudinal through-going fracture (sample B), and coal containing a lateral through-going fracture (sample C) are in the order of  $10^{-19} \text{ m}^2$ ,  $10^{-16} \text{ m}^2$ , and  $10^{-18} \text{ m}^2$ , respectively, which are within the range of values in the literature. The ratio of initial He permeabilities among sample A, sample B, and sample C is 1:1147:2 at a confining stress of 6 MPa under dry condition. Permeability changes little with the presence of a radial fracture across the sample. However,

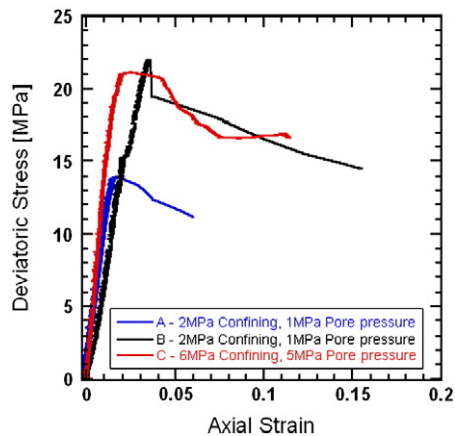


Fig. 12. Comparison of the strengths of three samples at 1 MPa effective confining pressure.

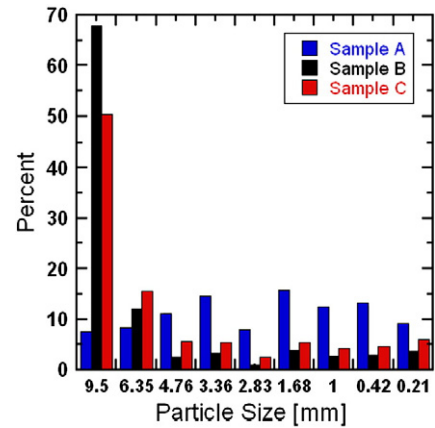


Fig. 13. Comparison of the post-failure particle size distribution of three samples at 1 MPa effective confining pressure.

the permeability increases by three orders of magnitude with a longitudinal fracture through the sample. This significant difference in permeability characterizes the nature of a coal seam composed of a matrix and cleat system in situ. This confirms that a typical coal seam, at the scale of meters, is a dual porosity dual permeability system. Therefore, the overall permeability range of a coal seam is primarily determined by the geometry of the fracture. For samples infiltrated with He, the rate of change of permeability is  $3.13 \text{ MPa}^{-1}$  for sample A and  $0.34^{-1}$  for sample B  $[(k_f - k_{in})/k_{in}\Delta P]$ , where  $k_f$ ,  $k_{in}$ , and  $\Delta P$  are the final permeability, initial permeability, and the change in pore pressure]. The large change in permeability for He with the longitudinal fracture causes the difference in permeability evolution for inert gas He. When sample A and sample C are injected with sorbing gases  $\text{CH}_4$  and  $\text{CO}_2$ , we observe that permeability first reduces at pore pressure below 3 MPa and then increases again when pore pressure is above 3 MPa. We postulate that for a system where swelling follows a Langmuir-type response, permeability declines at an early stage as sorption induced swelling controls the net permeability change, and the swelling rate gradually decreases with gas pressure and the influence of effective stress on permeability takes over at higher pressure. This phenomenon does not exist for sample B, where only permeability enhancement is found. This sample contains micro-fractures at the same intensity as the other samples (A and C) but the high permeability longitudinal fracture dominates the permeability response. The only difference between sample B and sample A is that the fracture walls are not connected by rock bridges in sample B. This observation implies that the presence of bridges across fractures in a crucial component in controlling the permeability evolution with pressure. The mechanistic rationale for this observation is that the fracture bridges importantly limit fracture deformation (Izadi et al., 2011). We suggest the crucial influence is in converting swelling strains into fracture closing strains – a feature that is no longer possible if the fracture halves are disconnected. This view is consistent with theoretical analysis of this response (Izadi et al., 2011).

At a confining pressure of 6 MPa and under dry condition, the amount of gas adsorbed in the longitudinally fractured coal (sample B) is 27.4% of that in coal containing small embedded fractures (sample A) for  $\text{CH}_4$  and 21.3% for  $\text{CO}_2$ . The swelling strain in sample B is 44.6% of that in sample A for  $\text{CH}_4$  and 71.9% for  $\text{CO}_2$ . The presence of a longitudinal through-going fracture changes the timing of the flow and hence changes the amount of sorption and swelling, which are time dependent processes. This contrast is well explained by a permeability model developed for coal containing discrete fractures (Izadi et al., 2011).

##### 4.2. The role of water-content

Coal, in situ is typically saturated (Gray, 1987), hence understanding the effect of water on the evolution of permeability, sorption, and

**Table 2**

Permeability, sorption, and swelling strain of coal in the literature.

Rank	Gas	Stress or temperature	Gas pressure [MPa]	Permeability [m <sup>2</sup> ]	Sorption	Swelling (%)	Authors
Bitu	N <sub>2</sub> , CH <sub>4</sub>	2–7 MPa		10 <sup>-18</sup> –10 <sup>-13</sup>	–	–	Somerton et al., 1975
Bitu	N <sub>2</sub>	8 MPa	2.8	10 <sup>-17</sup> –10 <sup>-13</sup>	–	–	Durucan and Edwards, 1986
Bitu	CH <sub>4</sub>	10 MPa	6.9	10 <sup>-18</sup>	–	0.4	Harpalani and Schraufnagel, 1990
Bitu, Subbi	CH <sub>4</sub> , CO <sub>2</sub>	7 MPa	5.3	10 <sup>-17</sup> –10 <sup>-13</sup>	–	2 (CO <sub>2</sub> ) 0.5 (CH <sub>4</sub> )	Robertson and Christiansen, 2005
–	CH <sub>4</sub> , CO <sub>2</sub>	8–26 MPa	4–23	10 <sup>-20</sup> –10 <sup>-17</sup>	–	0.15–0.6	Mazumder and Wolf, 2008
Bitu	Ar, CO <sub>2</sub>	7–20 MPa	4–10	10 <sup>-18</sup> –10 <sup>-15</sup>	–	–	Siriwardane et al., 2009
Bitu	N <sub>2</sub> , CO <sub>2</sub>	6–18 MPa	1–8	10 <sup>-18</sup> –10 <sup>-17</sup>	–	–	Wang et al., 2010b
Bitu	CH <sub>4</sub> , CO <sub>2</sub>	20 MPa	13	10 <sup>-16</sup> –10 <sup>-15</sup>	40 m <sup>3</sup> /ton (CO <sub>2</sub> ) 20 m <sup>3</sup> /ton (CH <sub>4</sub> )	2.4 (CO <sub>2</sub> ) 1.6 (CH <sub>4</sub> )	Pan et al., 2010
Anth	CH <sub>4</sub> , CO <sub>2</sub>	20 MPa	7	10 <sup>-21</sup> –10 <sup>-20</sup>	4.8 mmol/g (CO <sub>2</sub> ) 0.24 mmol/g (CH <sub>4</sub> )	–	Han et al., 2010
Bitu	CH <sub>4</sub> , CO <sub>2</sub>	30 °C	5	–	15–30 cm <sup>3</sup> /g (CO <sub>2</sub> ) 9–20 cm <sup>3</sup> /g (CH <sub>4</sub> )	–	Clarkson and Bustin, 1999
Bitu	CH <sub>4</sub> , CO <sub>2</sub>	22–45 °C	5–18	–	1.5 mmol/g (CO <sub>2</sub> ) 1.1 mmol/g (CH <sub>4</sub> )	–	Busch et al., 2003
Bitu	CH <sub>4</sub> , CO <sub>2</sub>	17 °C	2.8	–	20–25 m <sup>3</sup> /ton (CO <sub>2</sub> ) 4–6 m <sup>3</sup> /ton (CH <sub>4</sub> )	–	Mastalerz et al., 2004
Bitu	CH <sub>4</sub> , CO <sub>2</sub>	24–45 °C	7–10	–	17–29 ml/g (CO <sub>2</sub> ) 9–13 ml/g (CH <sub>4</sub> )	–	Harpalani et al., 2006
Bitu	CH <sub>4</sub> , CO <sub>2</sub>	40–60 °C	20	–	1.5–2 mmol/g (CO <sub>2</sub> ) 1–1.5 mmol/g (CH <sub>4</sub> )	–	Bae and Bhatia, 2006
Bitu	CH <sub>4</sub> , CO <sub>2</sub>	45–60 °C	19	–	2.04 mmol/g (CO <sub>2</sub> ) 1.23 mmol/g (CH <sub>4</sub> )	4 (CO <sub>2</sub> ) 2 (CH <sub>4</sub> )	Ottiger et al., 2008
Bitu	CH <sub>4</sub> , CO <sub>2</sub>	75 °C	1.8	–	1.4 mmol/g (CO <sub>2</sub> ) 0.45 mmol/g (CH <sub>4</sub> )	0.6	Kelemen and Kwiatek, 2009
Bi, semianth	CO <sub>2</sub>	45 °C	10	–	2.2 mmol/g (CO <sub>2</sub> , dry) 1.5 mmol/g (CO <sub>2</sub> , wet)	–	Siemons and Busch, 2007
Semianth	CH <sub>4</sub> , CO <sub>2</sub>	45–65 °C	4.1	–	2.04 mmol/g (CO <sub>2</sub> ) 0.94 mmol/g (CH <sub>4</sub> )	1.2	Battistutta et al., 2010
Bi, subbi, anth	CH <sub>4</sub> , CO <sub>2</sub>	35–55 °C	25	–	1.3–2.5 mmol/g (CO <sub>2</sub> ) 0.8–1.6 mmol/g (CH <sub>4</sub> )	–	Li et al., 2010
Bitu	CO <sub>2</sub>	25–55 °C	15	–	–	1.7–1.9	Day et al., 2008
Bitu	CH <sub>4</sub> , CO <sub>2</sub>	40 °C	8	–	–	0.94–1.81 (dry) 1.20–1.46 (wet)	van Bergen et al., 2009
Bitu	N <sub>2</sub> , CO <sub>2</sub>	40 °C 12 MPa	11	10 <sup>-18</sup> –10 <sup>-15</sup>	–	0.25–0.8	Kiyama et al., 2011
Bitu	CH <sub>4</sub> , CO <sub>2</sub>	25 °C 7 MPa	2	10 <sup>-15</sup>	–	0.18–0.36	Wang et al., 2010a
Bitu	CH <sub>4</sub> , CO <sub>2</sub>	25 °C	4	–	1.7–12 cm <sup>3</sup> /g	1.5–11	Czerw, 2011
Bitu	CH <sub>4</sub> , CO <sub>2</sub>	25 °C	4	–	–	0.5	Majewska et al., 2010

Note: Bitu stands for bituminous; Subbi stands for subbituminous, anth stands for anthracite; semianth stands for semi-anthracite.

swelling strain is a key need. The measured ratios of initial permeability between dry and wet samples for three samples are listed in Table 3. Generally, the presence of water reduces permeability by about one order of magnitude for samples without longitudinal fractures. With a longitudinal through-going fracture, permeability is decreased by about two orders with the presence of water, as shown for sample B.

For coal only containing small embedded fractures (sample A), different from the results under dry condition, we find the absence of permeability reduction with gas pore pressure when the sample is injected with CH<sub>4</sub> and CO<sub>2</sub>, as shown in Fig. 6(a). We speculate that the presence of water reduces the amount of gas adsorbed by 68% for CH<sub>4</sub> and by 69% for CO<sub>2</sub>. The water in the coal sample competes with the sorbing gases for adsorption sites and therefore reduces the sorption capacity. The swelling strain declines by 59% for CH<sub>4</sub> and 60% for CO<sub>2</sub>. We posit that the reduced sorption-induced swelling does not dominate the change in permeability through the whole gas pore pressure increasing process. Before injecting gas, the sample is water saturated. As gas pressure increases, the available water is gradually displaced by the injected gas, which also enhances the permeability over and above the reduction caused by swelling. This is confirmed by the observation that the rate of permeability increase in the wet sample using He is much larger than that for the sample under dry condition. However, the difference in final He permeabilities between dry and wet samples indicates that not all moisture can be removed by the injected He. We observe the same effect of water on permeability, sorption, and swelling on the longitudinally fractured coal (sample B) and the laterally fractured coal (sample C). So the rate of increase in permeability is

controlled both by the effective stress and the amount of water in the sample (89.4 MPa<sup>-1</sup> and 3.13 MPa<sup>-1</sup>).

#### 4.3. The relation between swelling strain and sorption

Coal swelling is likely to be related to the amount of gas adsorbed in coal, but the exact relation is unclear. The differences in the measured swelling strain of the coal when injected with different gases may therefore be related to the differences in the amount of gases adsorbed at different conditions. For the three samples tested in this study, the swelling is about 1.6 to 2.8 times higher for CO<sub>2</sub> than for CH<sub>4</sub> at a confining pressure of 6 MPa under dry conditions. It is about 1.4 to 2.5 times higher for CH<sub>4</sub> and CO<sub>2</sub> under dry conditions than under water-saturated conditions. These ratios are in good agreement with results reported in the literature.

We observe both roughly linear (coal containing small embedded fractures (sample A) at lower confining pressure and the laterally fractured coal (sample C)) and nonlinear (sample A at higher confining pressure and the longitudinally fractured coal (sample B)) relationships between the amount of gas adsorbed and swelling strain. For the nonlinearity in sample A, it starts with a linear relationship at lower gas pore pressure. As pore pressure increases, gas sorption slows but swelling continues, which has been observed in previous studies (Bustin, 2004; Levine, 1996). The reason may be due to the higher applied stress altering the pore structure of the coal and decreasing both sorption rate and swelling rate, but the reduction in sorption rate is larger than the reduction in swelling rate. Further investigation is needed to explain this phenomenon. The opposite behavior is also found in literature (Day et al., 2008), where swelling slows but adsorption continues.

For the nonlinear relationship observed in the longitudinally fractured coal (sample B) as shown in Fig. 9, almost perfect nonlinear curves are seen with a “swelling delay” in behavior. This measured coal swelling delay phenomenon may be explained by the dual porosity dual permeability characteristics of coal. Sorption and swelling begin in the vicinity of the vertical through-going fracture due to the much higher

**Table 3**

The ratios of initial permeability between dry and wet samples for three samples.

	He	CH <sub>4</sub>	CO <sub>2</sub>
Sample A	85	43	53
Sample B	214	458	264
Sample C	11	20	35

permeability of the fracture. But this local swelling may be small because it is rate-limited by diffusion into the matrix, even if it significantly alters the fracture permeability. As gas further penetrates the coal matrix the overall measured swelling strain builds. This logic is consistent with the observation that gas sorption and coal swelling is both anisotropic and heterogeneous (Karacan, 2003; Karacan, 2007; Karacan and Okandan, 2001). Thus, the relationship between gas sorption and swelling strain depends on the fracture geometry as well as the physical properties of the coal.

#### 4.4. The role of confining stress on permeability evolution

As apparent in Section 3, increasing confining pressure from 6 MPa to 12 MPa reduces the permeability by a factor of 14 for He, 11 for CH<sub>4</sub>, and 28 for CO<sub>2</sub>. It also leads to decline in the amount of gas adsorbed by 66% for CH<sub>4</sub> and 59% for CO<sub>2</sub>, and thus reduces the swelling strain for each gas. In addition to the universal effect of confining stress on the permeability evolution, our results confirm the conclusion that applied stress can reduce the sorption capacity and swelling strain of coal (Hol et al., 2011).

#### 4.5. The role of sorption on coal strength and structure

Previous observations have shown that CO<sub>2</sub> sorption may or may not have an impact on the mechanical strength of coal. In this study, we show that the sorption of CH<sub>4</sub> and CO<sub>2</sub> has a weakening effect. Under the same test condition, we find an 8 MPa compressive strength difference between coal containing small embedded fractures (sample A) and the longitudinally fractured coal (sample B) (22 MPa for sample B and 14 MPa for sample A). We would rationalize that sample A would have a larger strength since sample B had a longitudinal through-going fracture. The opposite outcome is consistent with a weakening effect due to gas sorption — this sample has been exposed to gas in its interior for about one-hundred times longer than for sample B. The post-failure sieve analyses show that the average particle size for sample B is three times larger than that of sample A. This may also imply the weakening effect of gas sorption. The laterally fractured coal (sample C) was broken at the same effective confining pressure (1 MPa) but with a higher confining pressure (6 MPa) to explore the effect of confining pressure on the strength. Results show that sample C has a larger strength than sample A consistent with a strengthening effect due to confining pressure. However, the strength of sample C is still lower than that of sample B that is again consistent with the weakening effect of sorption.

Since the coal is heterogeneous at a variety of length scales and the experiments are completed on one particular type (rank) of coal then these conclusions cannot necessarily be extended to all ranks. However, the principal features of the response are congruent with other observations and are anticipated to be broadly applicable.

## 5. Conclusions

We investigate the roles of fracture geometry and water-content on the evolution of the mechanical and transport characteristics for anthracite samples with three separate geometries — coal containing multiple small embedded fractures, coal containing a single longitudinal through-going fracture, and coal containing a single radial through-going fracture, under both dry and water-saturated conditions. The following conclusions can be drawn from this study.

- 1) The fracture geometry is of importance in understanding the evolution of permeability, sorption, and swelling. Not only can the fracture geometry change the magnitude of permeability by several orders of magnitude but it can also control the evolution of permeability, sorption, and swelling strain.
- 2) The presence of water similarly has the same role as fracture geometry. It can reduce the permeability by up to two orders of

magnitude. It also can alter the evolution of permeability, sorption, and swelling strain significantly.

- 3) In the case of the coal under investigation, a preferential sorption of CO<sub>2</sub> over CH<sub>4</sub> occurred is observed.
- 4) The relationship between the gas adsorbed and swelling strains can be either linear or nonlinear depending on the coal properties, stress conditions, and fracture geometry.
- 5) Applied stress can reduce the permeability, sorption, and swelling strain of coal.
- 6) CH<sub>4</sub> and CO<sub>2</sub> sorption is likely to have a weakening effect on the mechanical strength of coal.

## Acknowledgments

This work was funded by NIOSH under contract 200-2008-25702. This support is gratefully acknowledged.

## References

- Ates, Y., Barron, K., 1988. The effect of gas sorption on the strength of coal. *Mining Sci Technol* 6, 291–300.
- Bae, J.-S., Bhatia, S.K., 2006. High-pressure adsorption of methane and carbon dioxide on coal. *Energy Fuels* 20, 2599–2607.
- Bai, M., Elsworth, D., 2000. Coupled processes in subsurface deformation. ASCE Press, Flow and Transport. 336 pp.
- Battistutta, E., van Hemert, P., Lutyński, M., Bruining, H., Wolf, K.-H., 2010. Swelling and sorption experiments on methane, nitrogen and carbon dioxide on dry Selar Cornish coal. *International J. Coal Geology* 84, 39–48.
- Brace, W.F., Walsh, J.B., Frangos, W.T., 1968. Permeability of granite under high pressure. *J. Geophys. Res.* 73, 2,225–2,236.
- Busch, A., Gensterblum, Y., Krooss, B.M., 2003. Methane and CO<sub>2</sub> sorption and desorption measurements on dry Argonne premium coals: pure components and mixtures. *Int J. Coal Geology* 55, 205–224.
- Busch, A., Gensterblum, Y., Krooss, B.M., 2007. High-pressure sorption of nitrogen, carbon dioxide, and their mixtures on argonne premium coals. *Energy Fuels* 21, 1640–1645.
- Busch, A., Gensterblum, Y., Krooss, B.M., Siemons, N., 2006. Investigation of high-pressure selective adsorption/desorption behaviour of CO<sub>2</sub> and CH<sub>4</sub> on coals: An experimental study. *Int J. Coal Geology* 66, 53–68.
- Bustin, R.M., 2004. Acid gas sorption by British Columbia coal: implications for permanent disposal of acid gas in deep coal seams and possible co-production of methane. Final report OGC funding agreement 2000–16. The University of British Columbia.
- Chikatamarla, L., Cui, X., Bustin, R.M., 2004. Implications of volumetric swelling/shrinkage of coal in sequestration of acid gases 2004 International Coalbed Methane Symposium Proceedings. Tuscaloosa, Alabama paper. 0435.
- Clarkson, C.R., Bustin, R.M., 1999. The effect of pore structure and gas pressure upon the transport properties of coal: a laboratory and modeling study. 1. Isotherms and pore volume distributions. *Fuel* 78, 1333–1344.
- Cui, X., Bustin, R.M., Chikatamarla, L., 2007. Adsorption-induced coal swelling and stress: Implications for methane production and acid gas sequestration into coal seams. *J. Geophys. Res.* 112, B10202.
- Cui, X., Bustin, R.M., Dipple, G., 2004. Selective transport of CO<sub>2</sub>, CH<sub>4</sub>, and N<sub>2</sub> in coals: insights from modeling of experimental gas adsorption data. *Fuel* 83, 293–303.
- Cui, X.J., Bustin, R.M., 2005. Volumetric strain associated with methane desorption and its impact on coalbed gas production from deep coal seams. *AAPG Bulletin* 89 (9), 1181–1202.
- Czerw, K., 2011. Methane and carbon dioxide sorption/desorption on bituminous coal—Experiments on cubicoid sample cut from the primal coal lump. *Int J. Coal Geology* 85, 72–77.
- Day, S., Fry, R., Sakurovs, R., 2008. Swelling of Australian coals in supercritical CO<sub>2</sub>. *Int J. Coal Geology* 74, 41–52.
- Durucan, S., Edwards, J.S., 1986. The effects of stress and fracturing on permeability of coal. *Mining Sci Technol* 3, 205–216.
- Elsworth, D., Bai, M., 1992. Flow-deformation response of dual porosity media. *J. Geotechnical Eng* 118, 107–124.
- Goodman, A.L., Favors, R.N., Hill, M.M., Larsen, J.W., 2005. Structure Changes in Pittsburgh No. 8 Coal Caused by Sorption of CO<sub>2</sub> Gas. *Energy Fuels* 19, 1759–1760.
- Gray, I., 1987. Reservoir engineering in coal seams: Part 1. Phys process gas storage movement coal seams. *SPE Reservoir Eng* 2, 28–34.
- Gruskiewicz, M.S., Naney, M.T., Blencoe, J.G., Cole, D.R., Pashin, J.C., Carroll, R.E., 2009. Adsorption kinetics of CO<sub>2</sub>, CH<sub>4</sub>, and their equimolar mixture on coal from the Black Warrior Basin, West-Central Alabama. *Int J. Coal Geology* 77, 23–33.
- Han, F., Busch, A., van Wageningen, N., Yang, J., Liu, Z., Krooss, B.M., 2010. Experimental study of gas and water transport processes in the inter-cleat (matrix) system of coal: Anthracite from Qinshui Basin, China. *Int J. Coal Geology* 81, 128–138.
- Harpalani, S., Chen, G., 1997. Influence of gas production induced volumetric strain on permeability of coal. *Geotechnical Geological Eng* 15, 303–325.
- Harpalani, S., Prusty, B.K., Dutta, P., 2006. Methane/CO<sub>2</sub> sorption modeling for coalbed methane production and CO<sub>2</sub> sequestration. *Energy Fuels* 20, 1591–1599.
- Harpalani, S., Schraufnagel, R.A., 1990. Shrinkage of coal matrix with release of gas and its impact on permeability of coal. *Fuel* 69, 551–556.

- Hol, S., Peach, C.J., Spiers, C.J., 2011. Applied stress reduces the CO<sub>2</sub> sorption capacity of coal. *Int. J. Coal Geology* 85, 128–142.
- Hsieh, P.A., Tracy, J.V., Neuzil, C.E., Bredehoeft, J.D., Silliman, S.E., 1980. A transient laboratory method for determining the hydraulic properties of 'tight' rocks—I. Theory. *Int. J. Rock Mech. Min. Sci. Geomech. Abstr.* 18, 245–252.
- Huy, P.Q., Sasaki, K., Sugai, Y., Ichikawa, S., 2010. Carbon dioxide gas permeability of coal core samples and estimation of fracture aperture width. *Int. J. Coal Geology* 83, 1–10.
- Izadi, G., Wang, S., Elsworth, D., Liu, J., Wu, Y., Pone, D., 2011. Permeability evolution of fluid-infiltrated coal containing discrete fractures. *Int. J. Coal Geology* 85, 202–211.
- Karacan, C.O., 2003. Heterogeneous sorption and swelling in a confined and stressed coal during CO<sub>2</sub> injection. *Energy Fuels* 17 (6), 1595–1608.
- Karacan, C.O., 2007. Swelling-induced volumetric strains internal to a stressed coal associated with CO<sub>2</sub> sorption. *Int. J. Coal Geology* 72, 209–220.
- Karacan, C.O., Okandan, E., 2001. Adsorption and gas transport in coal microstructure: investigation and evaluation by quantitative X-ray CT imaging. *Fuel* 80, 509–520.
- Kelemen, S.R., Kwiatek, L.M., 2009. Physical properties of selected block Argonne Premium bituminous coal related to CO<sub>2</sub>, CH<sub>4</sub>, and N<sub>2</sub> adsorption. *Int. J. Coal Geology* 77, 2–9.
- Kiyama, T., Nishimoto, S., Fujioka, M., Xue, Z., Ishijima, Y., Pan, Z., Connell, L.D., 2011. Coal swelling strain and permeability change with injecting liquid/supercritical CO<sub>2</sub> and N<sub>2</sub> at stress-constrained conditions. *Int. J. Coal Geology* 85, 56–64.
- Larsen, J.W., 2004. The effects of dissolved CO<sub>2</sub> on coal structure and properties. *Int. J. Coal Geology* 57, 63–70.
- Levine, J.R., 1996. Model study of the influence of matrix shrinkage on absolute permeability of coalbed reservoirs. *Geological Soc Spec Publication* 109, 197–212.
- Li, D., Liu, Q., Weniger, P., Gensterblum, Y., Busch, A., Krooss, B.M., 2010. High-pressure sorption isotherms and sorption kinetics of CH<sub>4</sub> and CO<sub>2</sub> on coals. *Fuel* 89, 569–580.
- Liu, C.J., Wang, G.X., Sang, S.X., Rudolph, V., 2010. Changes in pore structure of anthracite coal associated with CO<sub>2</sub> sequestration process. *Fuel* 89, 2665–2672.
- Liu, H.H., Rutqvist, J., 2010. A new coal-permeability model: internal swelling stress and fracture-matrix interaction. *Transport Porous Media* 82 (1), 157–171.
- Majewska, Z., Ceglarska-Stefanska, G., Majewski, S., Zietek, J., 2009. Binary gas sorption/desorption experiments on a bituminous coal: Simultaneous measurements on sorption kinetics, volumetric strain and acoustic emission. *Int. J. Coal Geology* 77, 90–102.
- Majewska, Z., Majewski, S., Zietek, J., 2010. Swelling of coal induced by cyclic sorption/desorption of gas: Experimental observations indicating changes in coal structure due to sorption of CO<sub>2</sub> and CH<sub>4</sub>. *Int. J. Coal Geology* 83, 475–483.
- Mastalerz, M., Gluskoter, H., Rupp, J., 2004. Carbon dioxide and methane sorption in high volatile bituminous coals from Indiana, USA. *Int. J. Coal Geology* 60, 43–55.
- Mazumder, S., Wolf, K.H., 2008. Differential swelling and permeability change of coal in response to CO<sub>2</sub> injection for ECBM. *Int. J. Coal Geology* 74, 123–138.
- NIST, Thermochemical properties of fluid systems. <http://webbook.nist.gov/chemistry/fluid/>.
- Ottiger, S., Pini, R., Storti, G., Mazzotti, M., 2008. Competitive adsorption equilibria of CO<sub>2</sub> and CH<sub>4</sub> on a dry coal. *Adsorption* 14, 539–556.
- Palmer, I., Mansoori, J., 1998. How permeability depends on stress and pore pressure in coalbeds: a new model SPE 52607 SPE Reservoir Eval Eng 539–544 (Dec.).
- Palmer, I., Mansoori, J., 1996. How permeability depends on stress and pore pressure in coalbeds: a new model. SPE-52607.
- Pan, Z., Connell, L.D., Camilleri, M., 2010. Laboratory characterisation of coal reservoir permeability for primary and enhanced coalbed methane recovery. *International J. Coal Geology* 82, 252–261.
- Pappano, P.J., Mathews, J.P., Schobert, H.H., 1999. Structural determinations of Pennsylvania anthracites. *Am. Chem. Soc. Div. Fuel Chem.* 44 (3), 567–570.
- Pekot, L.J., Reeves, S.R., 2002. Modeling the effects of matrix shrinkage and differential swelling on coalbed methane recovery and carbon sequestration. U. S. Depart Energy DE-FC26-00NT40924.
- Pini, R., Ottiger, S., Burlini, L., Storti, G., Mazzotti, M., 2009. Role of adsorption and swelling on the dynamics of gas injection in coal. *J. Geophys. Res.* 114, B04203.
- Ranjith, P.G., Jasinge, D., Choi, S.K., Mehic, M., Shannon, B., 2010. The effect of CO<sub>2</sub> saturation on mechanical properties of Australian black coal using acoustic emission. *Fuel* 89, 2110–2117.
- Robertson, E.P., Christiansen, R.L., 2005. Measurement of sorption induced strain, Paper 0532, Proceedings of the 2005 International Coalbed Methane Symposium. Tuscaloosa, AL.
- Saghafi, A., Faiz, M., Roberts, D., 2007. CO<sub>2</sub> storage and gas diffusivity properties of coals from Sydney Basin, Australia. *Int. J. Coal Geology* 70, 240–254.
- Seidle, J.P., Huit, L.G., 1995. Experimental measurements of coal matrix shrinkage due to gas desorption and implications for cleat permeability increases. SPE-30010-MS.
- Shi, J.-Q., Durucan, S., 2004. A numerical simulation study of the Allison unit CO<sub>2</sub>-ECBM pilot: the impact of matrix shrinkage and swelling on ECBM production and CO<sub>2</sub> injectivity. Proceedings of 7th International Conference on Greenhouse Gas Control Technologies.
- Shi, J.-Q., Durucan, S., 2005. A model for changes in coalbed permeability during primary and enhanced methane recovery. *SPE Reservoir Eval Eng* 8 (4), 291–299.
- Shimada, S., Li, H., Oshima, Y., Adachi, K., 2005. Displacement behavior of CH<sub>4</sub> adsorbed on coals by injecting pure CO<sub>2</sub>, N<sub>2</sub>, and CO<sub>2</sub>-N<sub>2</sub> mixture. *Environ Geology* 49, 44–52.
- Siemons, N., Busch, A., 2007. Measurement and interpretation of supercritical CO<sub>2</sub> sorption on various coals. *Int. J. Coal Geology* 69, 229–242.
- Siriwardane, H., Haljasmaa, I., McLendon, R., Irdi, G., Soong, Y., Bromhal, G., 2009. Influence of carbon dioxide on coal permeability determined by pressure transient methods. *Int. J. Coal Geology* 77, 109–118.
- Somerton, W.H., Soylemezoglu, I.M., Dudley, R.C., 1975. Effect of stress on permeability of coal. *Int. J. Rock Mechanics Mining Sci Geomechanics Abstracts* 12, 129–145.
- van Bergen, F., Spiers, C., Floor, G., Bots, P., 2009. Strain development in unconfined coals exposed to CO<sub>2</sub>, CH<sub>4</sub> and Ar: Effect of moisture. *Int. J. Coal Geology* 77, 43–53.
- Viete, D.R., Ranjith, P.G., 2006. The effect of CO<sub>2</sub> on the geomechanical and permeability behaviour of brown coal: Implications for coal seam CO<sub>2</sub> sequestration. *Int. J. Coal Geology* 66, 204–216.
- Walker Jr., P.L., Verma, S.K., Rivera-Utrilla, J., Davis, A., 1988. Densities, porosities and surface areas of coal macerals as measured by their interaction with gases, vapours and liquids. *Fuel* 67, 1615–1623.
- Wang, G.X., Massarotto, P., Rudolph, V., 2009. An improved permeability model of coal for coalbed methane recovery and CO<sub>2</sub> geosequestration. *Int. J. Coal Geology* 77, 127–136.
- Wang, G.X., Wei, X.R., Wang, K., Massarotto, P., Rudolph, V., 2010a. Sorption-induced swelling/shrinkage and permeability of coal under stressed adsorption/desorption conditions. *Int. J. Coal Geology* 83, 46–54.
- Wang, S., Elsworth, D., Liu, J., 2010b. Evolution of permeability in coal to sorbing gases. A Preliminary Study. 44th U.S. Rock Mechanics Symposium. July 2010, Salt Lake City, Utah, 209.
- Wu, Y., Liu, J., Elsworth, D., Chen, Z., Connell, L., Pan, Z., 2010a. Dual poroelastic response of a coal seam to CO<sub>2</sub> injection. *Int. J. Greenhouse Gas Control* 4, 668–678.
- Wu, Y., Liu, J., Elsworth, D., Miao, X., Mao, X., 2010b. Development of anisotropic permeability during coalbed methane production. *J. Natural Gas Sci Eng* 2, 197–210.
- Zhang, H.B., Liu, J., Elsworth, D., 2008. How sorption-induced matrix deformation affects gas flow in coal seams: a new FE model. *Int. J. Rock Mechanics Mining Sci* 45 (8), 1226–1236.